Characterization of Surface Composition of Platinum and Ruthenium Nanoalloys Dispersed on Active Carbon

Sheng-Yang Huang, Shu-Min Chang, and Chuin-tih Yeh*

Department of Chemistry, National Tsing-Hua University, Hsinchu, Taiwan 30043, Republic of China

Received: August 29, 2005; In Final Form: October 1, 2005

Supported samples of 8 wt % monometallic Pt/C and Ru/C, as well as 12 wt % bimetallic $Pt_{50}Ru_{50}$/C, were prepared by the method of incipient wetness impregnation. Impregnated samples were subsequently reduced by hydrogen and then oxidized in air at different T_o temperatures. TEM and XRD examinations indicated that metal crystallites were finely dispersed with a diameter of $d_M \leq 3$ nm on the reduced samples. Reductive behavior of the oxidized samples by hydrogen was pursued with the technique of temperature programmed reduction (TPR). The temperature of the reduction peaks (T_r) noticed in the TPR profiles varied with the metal composition of catalysts and T_o temperature of oxidation. At $T_o = 300$ K, oxidation was confined to the surface layer of metallic crystallites. As a result, Pt^sO (with a peak at $T_r = 230$ K) or Pt^sO_2 ($T_r = 250$ K) was formed on monometallic Pt/C while Ru^sO_2 ($T_r \sim 380$ K) was formed on Ru/C. A reductive peak with $T_r = 250$ K was found from the bimetallic sample from $Pt_{50}Ru_{50}$/C oxidized at $T_o = 300$ K. The reductive peak suggests bimetallic crystallites were dispersed with cherry type structure, with Pt exposed at the surface and Ru in the core. On increasing the T_o temperature of oxidation treatment to 370 K and higher, T_r peaks between 270 and 350 K were gradually noticed on the oxidized bimetallic sample. Peaks in this T_r region are assigned to reduction of the oxidized alloy surface (A^sO). Evidently, a segregation of Ru to the surface of the bimetallic crystallites is indicated upon oxidation at $T_o > 380$ K.

Introduction

The fuel cell is regarded as a green technology for future energy. The proton exchange membrane fuel cell (PEMFC)[1,2] uses hydrogen gas as the fuel and platinum dispersed on active carbon (Pt/C) as the electrode catalyst. Hydrogen-rich gas (HRG) obtained from reformation of hydrocarbons is a fuel candidate for the anode for PEMFC. Besides CO_2, the reformed HRG is generally contaminated with a small fraction of CO.[3] The CO tends to adsorb strongly on the surface of platinum crystallites and poison Pt/C electrodes on the anode of PEMFC. The poison effect may be partially relieved by alloying the Pt/C catalyst with ruthenium.[4−7] Ru/C alone is inactive at the anode. The role of Ru in Pt−Ru bimetallic catalysts on the suppression of CO poison has been attributed to two reasons: the electronic effect and the bifunctional effect.[8−11]

Pt−Ru/C has been extensively explored as the anode catalyst for PEMFC. Pt and Ru with a metallic composition from $Pt_{30}Ru_{70}$ to $Pt_{100}Ru_0$ (where the numbers subscript to the metals indicate their atomic percentage)[12,13] were finely dispersed as alloy crystallites on active carbon. The size of dispersed crystallites may be characterized with TEM and XRD. Generally, an average crystalline size of $d \leq 3$ nm was prepared for bimetallic catalysts used in the anode of PEMFC.

Figure 1 describes two hypothetic hemisphere models for $Pt_{50}Ru_{50}$ crystallite. They have the same diameter of $d_c = 2.2$ nm but with different atom distributions. The model on top indicates a homogeneously distributed alloy while that at the bottom presents a cherry-type crystallite with Pt atoms at the surface and Ru atoms in the core. From this model, we know the following information:

1. Each hemispheric crystallite contains ∼100 atoms with an atomic diameter of 0.26 nm.[14−16]
2. Eight atoms may be lined up along the diameter of the crystallite.
3. The dispersion (fraction of metal exposed to surface) of atoms in these two crystallites is around $D \sim 0.5$.

The catalytic activity of prepared $Pt_{50}Ru_{50}$/C should vary with the surface composition of alloy crystallites dispersed. The surface composition of solid samples can usually be characterized with X-ray photoelectron spectroscopy (XPS) and Auger electron spectroscopy (AES). Unfortunately, the escaping depth of the electron ($\lambda \sim 3$ nm)[17] prevents these techniques from giving a decent characterization of the surface composition of alloy crystallites with a diameter <3 nm. However, the surface composition of alloy crystallites may be explored by the technique of temperature programmed reduction (TPR).

Upon calcination treatments, surface platinum (Pt^s) on reduced Pt crystallites is oxidized to Pt^sO and Pt^sO_2, i.e.,

$$2Pt^s + O_2 \rightarrow 2Pt^sO \quad (1)$$

$$Pt^s + O_2 \rightarrow Pt^sO_2 \quad (2)$$

The state of Pt^sO_x may be characterized with the TPR technique. In the characterization, metal oxides were reduced by flowing hydrogen,

$$MO_x + xH_2 \rightarrow xH_2O + M \quad (3)$$

The oxidation state of platinum in PtO_x can be quantitatively determined from the stoichiometry of hydrogen consumed in TPR. In our laboratory, Pt^sO_x formed in reactions 1 and 2 has been extensively characterized for different platinum catalysts

* To whom correspondence should be addressed. E-mail: ctyeh@mx.nthu.edu.tw. Fax: 886-3-5726047.

10.1021/jp054870k CCC: $33.50
Published on Web 12/14/2005

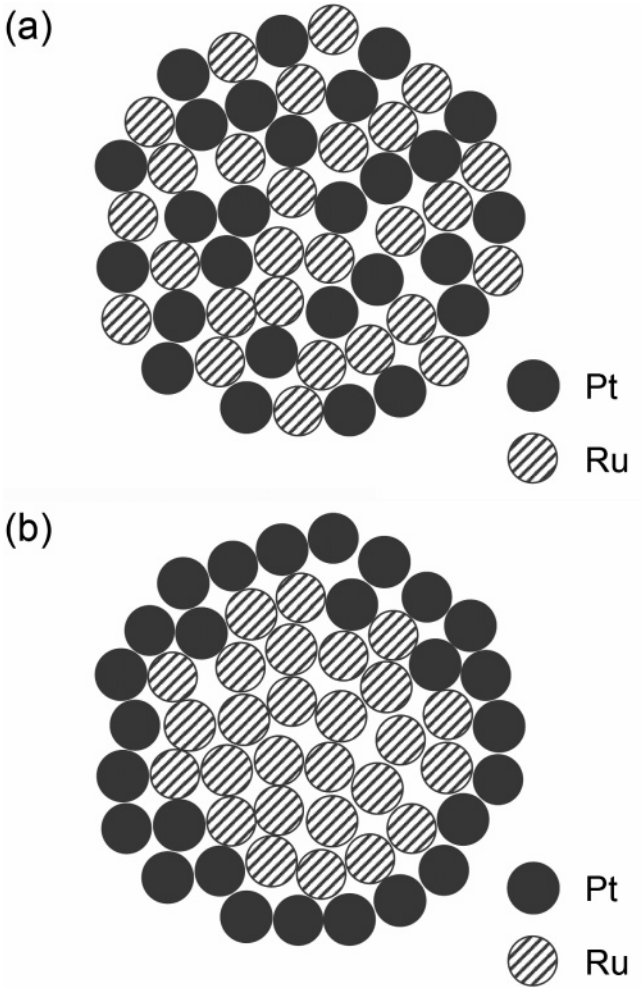

Figure 1. Models for two theoretical hemisphere $Pt_{50}Ru_{50}$ crystallites with a diameter of $d_c = 2.2$ nm but different atom distributions. The model on top indicates a homogeneously distributed alloy while that at the bottom presents a cherry-type crystallite with Pt atoms exposed at the skin while Ru atoms stay in the core.

TABLE 1: Variation in TPR Peak Temperatures of Species Pt^sO and Pt^sO_2 for Pt Crystallites Dispersed on Different Supports

	T_r/K		
sample	Pt^sO	Pt^sO_2	ref
Pt/zeolite channel	350	390	18
Pt/Al_2O_3	320	370	19
Pt/CeO_2	260	290	20
Pt/SiO_2	220	270	21
Pt/C	230	250	this study

with TPR. Experimental T_r temperature varies with the dispersing support and the stoichiometry x. Table 1 lists the T_r temperature of Pt^sO_x dispersed on different supports (Al_2O_3, CeO_2, SiO_2, and mordenite). Observed T_r varies from 220 to 390 K, dependent on the kind of support and the oxidation state of PtO_x.

Table 2 summarizes the literature reports on TPR of supported ruthenium catalysts. Upon calcination treatment at $T_o > 370$ K, calcined Ru catalyst always shows a reduction peak in the T_r range between 330 and 470 K in TPR. This peak was assigned to the reduction of RuO_2. The variation in T_r of RuO_2 was attributed to the type of dispersed support and calcination temperature.

In this paper we want to report that oxidation of Pt−Ru alloy crystallites is confined to their surface upon calcination at ambient temperature. The reduction temperature of their surface oxidized at ambient temperature varies with the surface composition of alloy crystallites. As a consequence, the surface composition of bimetallic crystallites dispersed on Pt−Ru/C catalysts may be probed with the TPR technique.

TABLE 2: Literature Review on the Characterization of RuO_2 on Supported Ruthenium Catalysts by Temperature Program Reduction

sample	T_o/K	T_r/K	ref
RuO_2, standard		380	22
4% Ru/Al_2O_3	770	470	23
2% Ru/SiO_2	770	420	24
5% Ru/SiO_2	470	450	25
6% Ru/CeO_2	470−870	330−380	22
3% Ru/SiO_2	370−770	360−410	26
8% Ru^sO_2/C	320−470	370	this study
8% Ru^cO_2	570	450	this study

TABLE 3: Physical Properties Characterized for Samples Freshly Prepared in this Study

	metal wt %		particle size/nm	
catalyst	Pt	Ru	TEM	XRD
Pt/C-H620	7.7		2.3	2.0
Ru/C-H620		7.1	2.3	2.1
$Pt_{50}Ru_{50}$/C-H620	7.4	3.7	2.1	2.4[a]

[a] $Pt_{50}Ru_{50}$/C-H1000.

Experimental Section

A. Sample Preparation. Supported samples of 8 wt % Pt/C (hereafter referred to as Pt/C), 8 wt % Ru/C (Ru/C), and 12 wt % PtRu/C (8 wt % Pt and 4 wt % Ru, i.e., $Pt_{50}Ru_{50}$/C) were prepared by the incipient wetness impregnation method. Powders of commercial carbon black (Vulcan XC72, SA = 230 $m^2\ g^{-1}$) were impregnated with an aqueous solution of $PtCl_4$ (Merck) and/or $RuCl_3 \cdot 3H_2O$ (Strem). Impregnated powders were subsequently dried at 320 K for 24 h, reduced under flowing H_2/N_2 (10/90 v/v) gas for 1 h at 620 K, and stored as fresh catalysts. Table 3 lists the physical properties characterized for samples freshly prepared in this study.

B. Sample Characterization. Freshly prepared catalysts have been characterized by X-ray diffraction (XRD, MAC Science MXP18, at 40 kV and 100 mA), analytic electron microscopy (AEM, JEOL JEM-2010, 200 kV), and TPR. In each TPR study, a fresh sample of 50 mg was inserted into a U-shaped TPR cell, preoxidized at a predetermined temperatures (T_o ranged from 300 to 570 K), flushed with N_2 at 300 K, and then reduced by a flow of 10% H_2 in N_2 on raising the TPR temperature from 190 to 500 K at a rate of 7 K min^{-1}.

Results and Discussion

A. Characterization of Monometallic Pt/C Samples. Figure 2 compares the TEM micrograph of 8% Pt/C samples of Pt/C-H620 (freshly reduced at $T_R = 620$ K) and Pt/C-H620-O570 (with an additionally oxidation treatment in air at $T_o = 570$ K). Pt particles are found, in Figure 2a, finely dispersed on the freshly reduced Pt/C-H620. The average size of Pt particles in the sample is $d_{Pt} = 2.3 \pm 1.0$ nm, according to the attached histogram analysis. Most of Pt particles in the oxidized Pt/C-H620-O570 were unaffected by the calcinations and retained a $d_{Pt} \sim 2.3$ nm of Pt/C-H620. However, a small fraction of Pt particles on the sample was aggregated to $d_{Pt} \sim 7.0$ nm after the oxidation treatment at $T_o = 570$ K (Figure 2b).

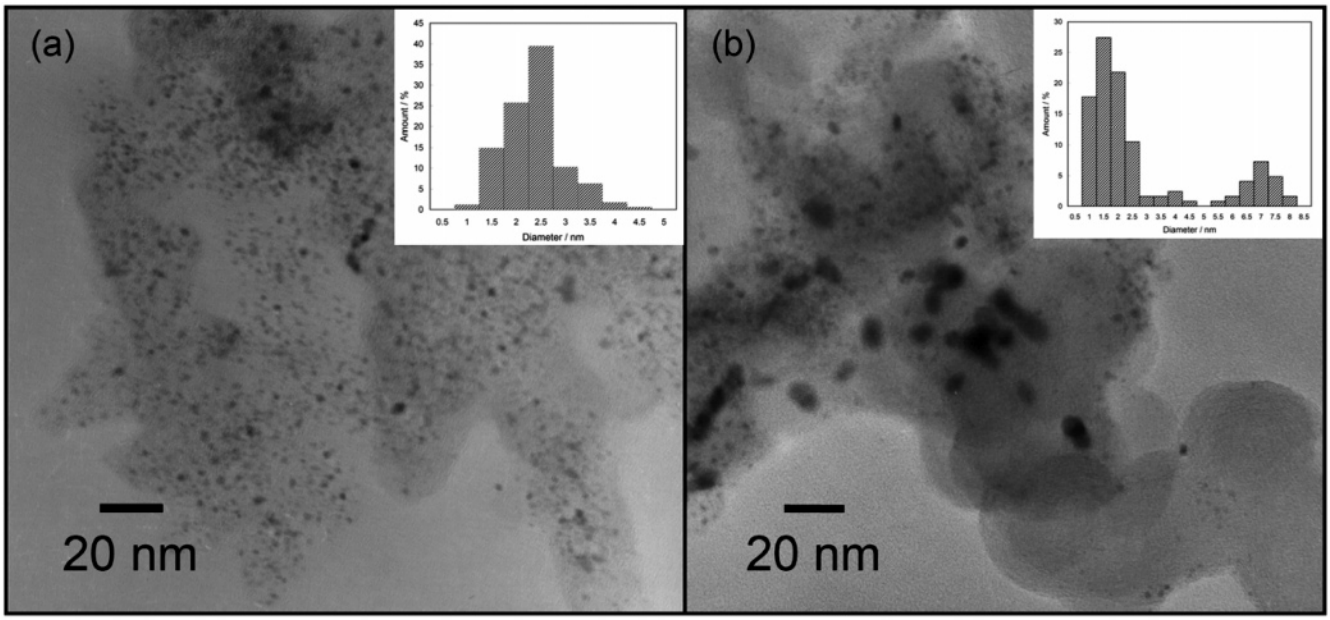

Figure 2. TEM micrograph of 8% Pt/C samples: (a) freshly reduced at $T_r = 620$ K (Pt/C-H620) and (b) after calcination at $T_o = 570$ K (Pt/C-H620-O570) by air. The average sizes of Pt particles are d_{Pt} = (a) 2.3 and (b) 2.7 nm.

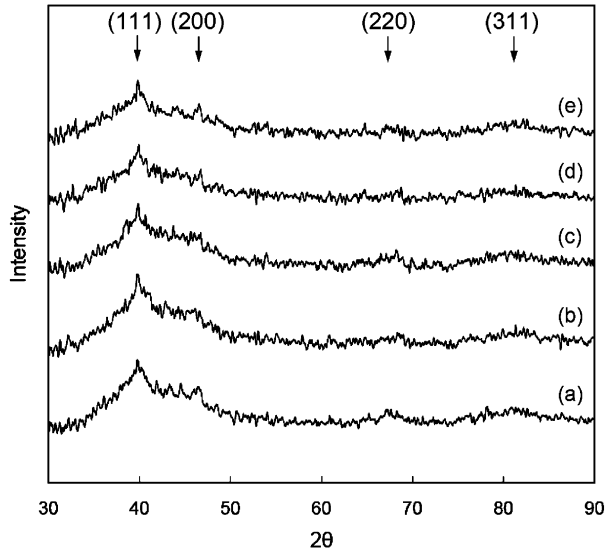

Figure 3. Effect of calcinations temperature on XRD of Pt/C-H620: (a) without calcination, $d_{Pt} = 2.0$ nm; (b) $T_o = 300$ K, $d_{Pt} = 2.1$ nm; (c) $T_o = 370$ K; (d) $T_o = 470$ K; and (e) $T_o = 570$ K.

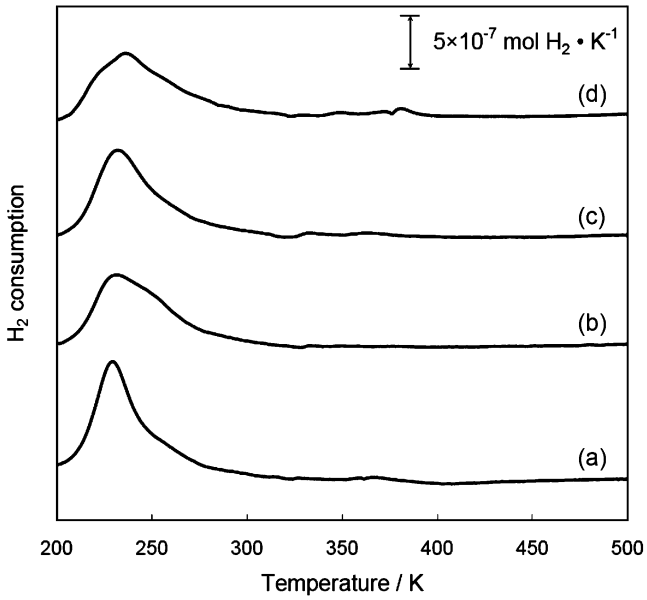

Figure 4. TPR spectra from Pt/C-H620-O_x. The reduced Pt/C-H620 sample has been reoxidized at T_o = (a) 300, (b) 370, (c) 470, and (d) 570 K. The area of the reduction peak has been used to estimate hydrogen consumption of N_{H2}/N_{Pt} = (a) 0.60, (b) 0.62, (c) 0.66, and (d) 0.61.

Active carbon is a high surface area support and tends to be oxidized at elevated temperature in air. Upon disposition of platinum crystallites, the oxidation of this support was significantly promoted by a spillover of oxygen through the active Pt. A loss in the weight of Pt/C catalyst generally occurred on calcination treatments of Pt/C catalysts. The aggregation of Pt found in Figure 2b should have been caused by a loss of surface area of carbon support by the O_2 spillover.

The sample of Pt/C-H620 has been divided into several portions to study the effects of oxidation treatment. Figure 3 presents XRD traces from fresh Pt/C and samples of Pt/C-H620-T_o. Four Pt peaks, (111), (200), (220), and (311), were noticed at $2\theta = 39°$, 46°, 67°, and 81°, respectively. The average particle size of Pt crystallites on these samples may be calculated as $d_{Pt} = 2.0$ nm, using the Debye−Scherrer equation. The calculated d_{Pt} is in good agreement with the small Pt particles of 2.3 ± 1.0 nm found from TEM.

Figure 4 presents a series of TPR traces from Pt/C-H620-O_x samples oxidized in a T_o temperatures range of 300 to 570 K. Each trace contains a reduction peaked at $T_r \sim 230$ to 250 K. On comparing to TPR results of other platinum samples (Table 1), T_r of Pt^sO_x dispersed on active carbon is similar to those dispersed on supports of CeO_2 and SiO_2.

The dispersion of Pt may be estimated from the ratio in number of hydrogen consumption in reduction per platinum atom ($R_{H2} = N_{H2}/N_{Pt}$). The ratio R_{H2} has been quantitatively calculated for each trace in Figure 4. For the sample oxidized at $T_o = 300$ K, a reductive peak at $T_r = 230$ K with $R_{H2} = 0.60$ was found. The R_{H2} indicated a dispersion of $D_{Pt} \sim 0.6$ according to the stoichiometry of reaction 1. A shoulder peak at $T_r = 250$ K was additionally found in the TPR trace of

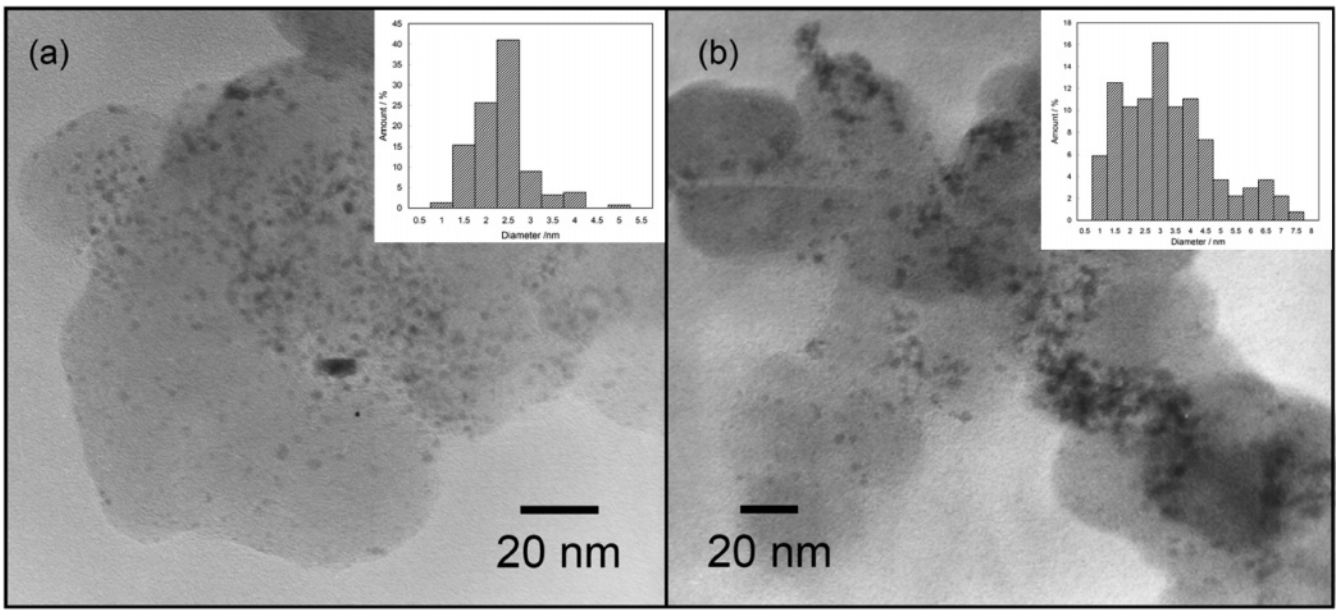

Figure 5. TEM micrographs of Ru/C-H620 and Ru/C-H620-O570. The average sizes of Ru particles are d_{Ru} = (a) 2.3 and (b) 3.2 nm.

Pt/C-H620-O470 and R_{H2} was increased slightly to 0.7. Probably, a portion (~10%) of Pt^s was oxidized to Pt^sO_2 upon severe oxidation at T_o = 470 K:

$$2Pt^s + xO_2 \rightarrow 2Pt^sO_x \quad (4)$$

where x is a number between 1 and 2. Equation 4 therefore represents a combination of reactions 1 and 2.

B. Characterization of Monometallic Ru/C Samples. Figure 5 compares the TEM micrographs of Ru/C-H620 and Ru/C-H620-O570. Ru particles on the fresh Ru/C-H620 have a size of $d_{Ru} = 2.0 \pm 1.0$ nm according to the histogram analysis (Figure 5a). Evidently, ruthenium was homogeneously dispersed on the support of Vulcan XC-72 carbon. After an oxidation treatment at 570 K, some of Ru particles on Ru/C-H620 retained a size of 2 nm. A large fraction of them were aggregated to $d > 3$ nm.

The sample of Ru/C-H620 has also been divided into several portions to study the effects of calcination temperature on physical and reductive properties. Figure 6 presents the XRD traces from Ru/C-H620 and Ru/C-H620-O_x. Samples of Ru/C-H620 and Ru/C-H620-O370 showed a peak at $2\theta = 44°$, which is characteristic of Ru (101). The peak of metallic Ru was replaced by (101) and (211) peaks of RuO_2 (at $2\theta = 35$ and 54, respectively) after a severe calcination of the Ru/C-H620 at $T_o > 520$ K (Figure 6, traces d and e). Under such calcination, oxygen should have diffused into the bulk of Ru particles and formed Ru^cO_2 (crystalline ruthenium dioxide), i.e.,

$$Ru + O_2 \rightarrow Ru^cO_2 \quad (5)$$

Figure 7 presents a series of TPR traces from Ru/C-H620 sample calcined at different T_o. A reductive peak was found in trace from each calcined sample. Their peak position (T_r), however, varied with the T_o of the oxidation treatment. A peak at T_r = 370 and 450 K was found in traces a to c in Figure 7 (with low T_o) and trace d in Figure 7 (T_o = 570 K), respectively. XRD characterization has found that Ru has been oxidized to Ru^cO_2 (reaction 5) at $T_o > 570$ K. Accordingly, the peak at T_r = 450 K was assigned to reduction of Ru^cO_2:

$$Ru^cO_2 + 2H_2 \rightarrow Ru + 2H_2O \quad (6)$$

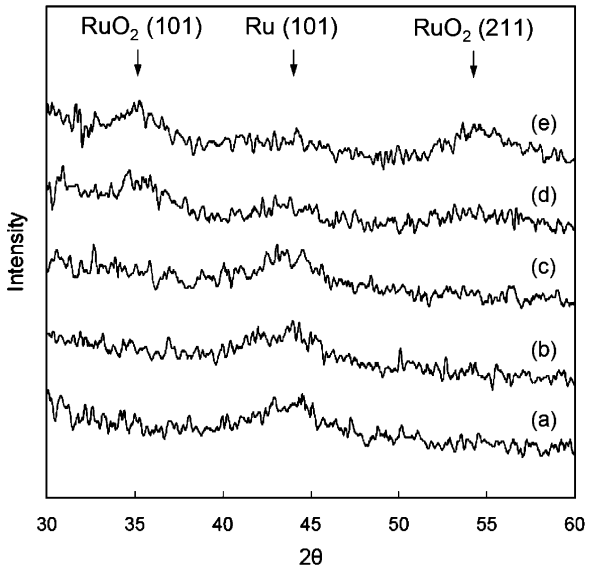

Figure 6. XRD traces from Ru/C-H620 (a) and Ru/C-H620-O_x with T_o = (b) 300, (c) 370, (d) 520, and (e) 570 K.

while the peak at T_r = 370 K was assigned to reduction of amorphous RuO_2 (Ru^aO_2) oxidized at low oxidation treatment:

$$Ru^aO_2 + 2H_2 \rightarrow Ru + 2H_2O \quad (7)$$

The hydrogen consumption ($R_{H2} = N_{H2}/N_{Ru}$) in TPR traces in Figure 7 has been quantitatively determined. The consumption was calculated as R_{H2} = 1.0 for samples oxidized at low temperatures of T_o = 300 and 370 K. Evidently, the mild oxidation at $T_o < 370$ K was limited to chemisorption of oxygen on dispersed Ru crystallites on knowing the dispersion of Ru on Ru/H620 was $D_{Ru} \sim 0.5$. Calculated consumption increased with T_o temperature and reached R_{H2} = 2.0 at T_o = 570 K. The increase in hydrogen consumption indicates a diffusion of oxygen to the subsurface of Ru at high T_o. The extensive diffusion and oxidation upon $T_o > 570$ K formed crystalline Ru^cO_2.

JCPDS data indicate that RuO_2 belongs to the tetragonal structure and Ru metal is in the hcp structure. Probably, crystalline RuO_2 formed at 470 K on oxidation of Ru crystals

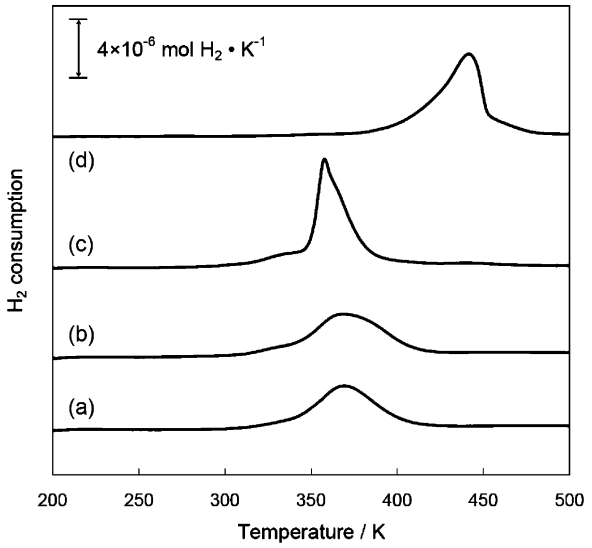

Figure 7. TPR spectra of Ru/C-H620-O_x, with T_o = (a) 300, (b) 370, (c) 470, and (d) 570 K. Calculated hydrogen consumption is N_{H2}/N_{Ru} = (a) 1.36, (b) 1.50, (c) 2.08, and (d) 2.02.

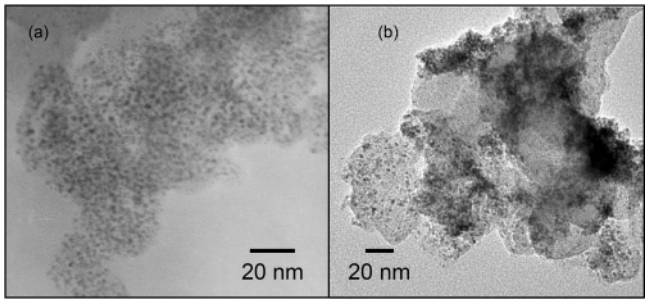

Figure 8. TEM micrographs of $Pt_{50}Ru_{50}$/C-H620 and $Pt_{50}Ru_{50}$/C-H620-O570. The average sizes of Pt−Ru alloy particles are d_{PtRu} = (a) 2.1 and (b) 2.5 nm.

was in a metastable structure other than the normal tetrahedral. This metastable structure will convert into a stable tetragonal structure upon oxidation at $T_o \geq 570$ K. This metal stable state has a lower (Figure 7c) T_r temperature than either amorphous ruthenium oxide (Figure 7a,b) or tetrahedral RuO_2 (Figure 7d).

C. Characterization of Bimetallic Pt−Ru/C Samples. Figure 8 compares the TEM micrographs of $Pt_{50}Ru_{50}$/C-H620 and $Pt_{50}Ru_{50}$/C-H620-O570. Pt and Ru were found homogeneously deposited as finely dispersed alloy particles in these samples. The average sizes of the alloy particles are d_{PtRu} = 2.1 ± 1.0 nm (Figure 8a) for $Pt_{50}Ru_{50}$/C-H620 and 2.4 ± 1.0 nm (Figure 8b) for $Pt_{50}Ru_{50}$/C-H620-O570. Comparing to results in Figures 2b and 5b, alloy particles of Pt−Ru on supported $Pt_{50}Ru_{50}$/C exhibited a higher resistance to aggregation than the individual monometallic samples of Pt/C and Ru/C upon oxidation treatment.

Figure 9 presents the XRD traces from samples of fresh $Pt_{50}Ru_{50}$/C-H620 and $Pt_{50}Ru_{50}$/C-H620-O_x. Trace a of fresh $Pt_{50}Ru_{50}$/C-H620 did not show any peak at $2\theta = 44°$ expected for hcp Ru (101) but had a faint broad peak around 40° which may be attributed to (111) diffraction from small crystallites of the fcc phase of Pt-rich (A^{Pt}) alloy. Upon calcination treatment at low temperatures of $T_o < 470$ K, the intensity of this peak decreased (Figure 9, traces b to d). Probably the surface of the alloy particles was oxidized and the metal portion had therefore shrunk to the core of the particles. Upon calcinations at $T_o >$ 520 K (Figure 9, traces e and f) two sharp peaks at $2\theta = 35°$ and 54° were observed from $Pt_{50}Ru_{50}$/C-H620-O_x. These sharp

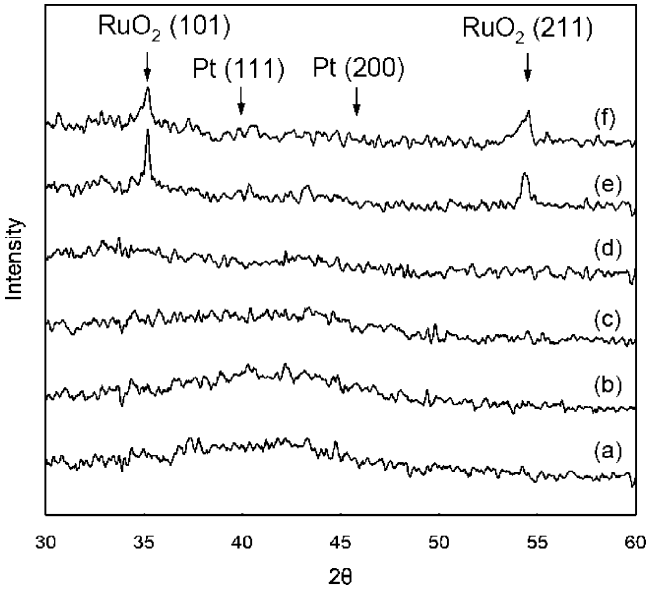

Figure 9. XRD traces from $Pt_{50}Ru_{50}$/C-H620 (a) and $Pt_{50}Ru_{50}$/C-H620-O_x with T_o = (b) 300, (c) 370, (d) 470, (e) 520, and (f) 570 K.

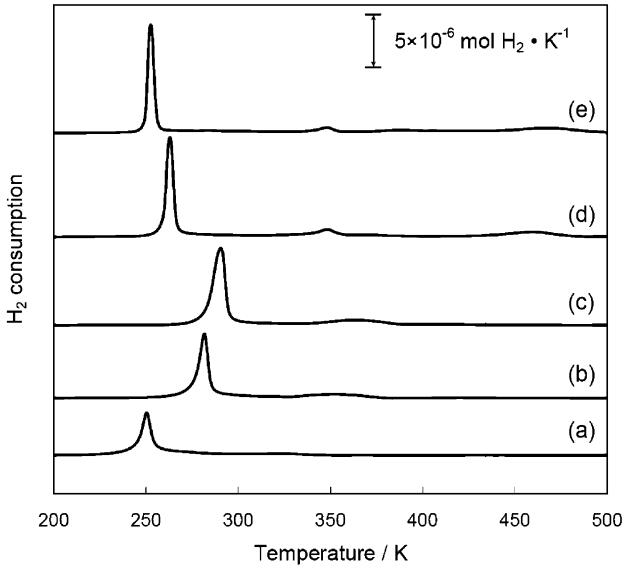

Figure 10. TPR spectra of $Pt_{50}Ru_{50}$/C-H620−O_x with T_o = (a) 300, (b) 370, (c) 470, (d) 520, and (e) 570 K. The $N_{H2}/N_{(Pt+Ru)}$ is (a) 0.64, (b) 0.84, (c) 1.03, (d) 1.17, and (e) 1.17.

peaks have been assigned to (101) and (211) diffractions of Ru^cO_2.[27] Evidently, Ru had been segregated out of the alloy particles and then aggregated as large Ru^cO_2 crystallites at severe oxidations of $T_o > 520$ K.

Figure 10 presents a series of TPR traces from the fresh $Pt_{50}Ru_{50}$/C-H620 alloy sample oxidized at different T_o temperatures. The $Pt_{50}Ru_{50}$/C-H620-O300 exhibited a sharp peak at $T_r = 250$ K. The position of this peak is quite close to the T_r of Pt^sO_x in Pt/C (230−250 K established in Table 1). Conceivably, bimetallic particles on the fresh $Pt_{50}Ru_{50}$/C-H620 should have covered the platinum surface. The trace suggested that the Pt−Ru alloy particles on PtRu/C reduced at 620 K may have a cherry-like structure (see Figure 1b) with Pt atoms on the surface and Ru atoms in the core.

On increasing the temperature of calcination treatment to $T_o >$ 470 K, the reduction peak gradually shifted to 290 K (traces b and c of Figure 10). The T_r position of these reduction peaks locates between those of Pt^sO_2 (250 K) and Ru^sO_2 (370 K). Peaks in Figure 10 may be attributed to a reduction of alloy

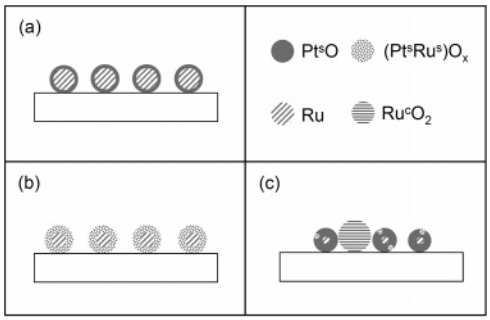

Figure 11. The segregation and migration of Pt−Ru alloy particles upon calcination treatment at T_o = (a) 300, (b) 370 and 470, and (c) 520 and 570 K.

oxides (AO_x), with different Pt−Ru composition, formed on the surface layer of alloy crystallites, i.e.,

$$AO_x + xH_2 \rightarrow A + xH_2O \qquad (8)$$

Evidently, ruthenium in the core of cherry crystallites of Pt−Ru should have segregated to the surface upon oxidation treatment at $T_o > 370$ K. The segregation may be conceivable from the knowledge that Ru has a higher tendency to bond with oxygen than Pt. The peak position for reaction 8 should vary with the composition of alloy. The oxide of the platinum-rich alloy ($A^{Pt}O$) should have $T_r \sim 250$ K. The reduction temperature of alloy oxide increases with the composition of ruthenium and approaches $T_r = 370$ K for $A^{Ru}O$ (oxide for ruthenium-rich alloy).

The peak for $A^{Pt}O$ reduction shifted from $T_r = 250$ to 290 K (traces a to c in Figure 10) on raising T_o to 470 K. The shift may be attributed to an increase in the extent of Ru segregation. On increasing the temperature of oxidation treatment to $T_o >$ 520 K (traces d and e in Figure 10), two weak reduction peaks at $T_r = 350$ and 460 K appeared besides the major peak of $A^{Pt}O_x$ reduction at $T_r = 250$ K. These weak peaks may be assigned for reduction of A^RO_x (surface-Ru-rich alloy phase, $T_r = 350$ K) and Ru^cO_2 (reaction 6), respectively. These two species must have been produced through excess Ru segregation during oxidation. It is noteworthy that a formation of Ru^cO_2 in sample $Pt_{50}Ru_{50}$/C upon oxidation treatment at $T_o > 570$ K has already been suggested in XRD traces in Figure 9.

D. Model for $Pt_{50}Ru_{50}$/C Oxidation. Figure 11 provides a schematic model for the Ru segregation and the aggregation of Pt−Ru alloy particles upon oxidation of sample $Pt_{50}Ru_{50}$/C-H620 treatment. The Pt−Ru alloy particles on the reduced PtRu/C-H620 were deposited as cherry-type crystallite with Pt atoms at the surface and Ru atoms in the core (Figure 1b). Upon adsorption of oxygen at $T_o = 300$ K, the Pt surface of alloy crystallites was oxidized as a Pt^sO layer (Figure 11a). Upon mild oxidation ($T_o = 370-470$ K), a portion of Ru segregated by oxygen to the surface of crystallites to form $A^{Pt}O_x$ (Figure 11b). The extent of segregation increased with oxidation temperature. On severe oxidation at $T_o \geq 520$ K, A^{Ru} and crystalline Ru^cO_2 structure were formed due to the enhanced Ru segregation (Figure 11c).

According to the model in Figure 11, the surface composition of Pt−Ru alloy crystallites on the fresh $Pt_{50}Ru_{50}$/C-H620 sample was covered by a surface shell of Pt atoms. However, the surface of alloy crystallites may be enriched with Ru by segregation through appropriate calcination treatment. We have demonstrated in this report that the extent of segregation may be controlled by the condition of treatment and monitored by the TPR technique. The catalytic activity of alloy catalyst depends heavily on the surface composition of their dispersed alloy particles. It is our plan to pursue the activity of alloy particles on PtRu/C catalyst with their surface composition characterized by the TPR technique developed in this study.

Conclusions

Samples of 8 wt % Pt/C, 8 wt % Ru/C, and 12 wt % of $Pt_{50}Ru_{50}$/C have been prepared by the incipient wetness impregnation method and exhibit a metal dispersion around $D = 50\%$. The technique of TPR can be used to characterize the surface composition of Pt−Ru alloy particles deposited on active carbon. The following observations have been noticed in this study:

1. Pt and Ru may be dispersed on active carbon as nanosized (3 nm or less) metallic particles by the incipient wetness method.

2. Upon an oxidation treatment at ambient temperature, metal atoms on the surface of the dispersed Pt, Ru, and Pt−Ru alloy crystallites were oxidized to Pt^sO and Ru^sO_2 or AO_x.

3. The temperature required for the reduction (T_r) of these surface oxides differed with their composition. Pt^sO and Ru^sO_2 exhibited a T_r at 230 and 370 K while the T_r of the AO stayed between 230 and 370 K and varied with the composition of A.

4. The TPR technique may be used to probe the surface composition of Pt−Ru alloy crystallites.

Acknowledgment. The authors thank the National Science Council and the Education Ministry of the Republic of China for their financial support of this study.

References and Notes

(1) Hogarth, M. P.; Ralph, T. R. *Platinum Met. Rev.* **2002**, *46*, 146.
(2) Ralph, T. R.; Hards, G. A. *Chem. Ind.* **1998**, *9*, 337.
(3) Mo, L.; Zheng, X.; Yeh, C. T. *Chem. Commun.* **2004**, 1426.
(4) Stonehart, P.; Ross, P. N. *Catal. Rev. Sci. Eng.* **1975**, *12*, 1.
(5) Liu, R.; Iddir, H.; Fan, Q.; Hou, G.; Bo, A.; Ley, K. L.; Smotkin, E. S. *J. Phys. Chem. B* **2000**, *104*, 2518.
(6) Lin, W. F.; Zei, M. S.; Eiswirth, M.; Ertl, G.; Iwasita, T.; Vielstich, W. *J. Phys. Chem. B* **1999**, *103*, 6968.
(7) Long, J. W.; Stroud, R. M.; Swider-Lyons, K. E.; Rolison, D. R. *J. Phys. Chem. B* **2000**, *104*, 9772.
(8) Park, K.-W.; Choi, J.-H.; Lee, S.-A.; Pak, C.; Chang, H.; Sung, Y.-E. *J. Catal.* **2004**, *224*, 236.
(9) Watanabe, M.; Motoo, S. *J. Electroanal. Chem.* **1975**, *60*, 275.
(10) Toda, T.; Igagrashi, H.; Uchida, H.; Watanabe, M. *J. Electrochem. Soc.* **1999**, *146*, 3750.
(11) Park, K.-W.; Choi, J.-H.; Sung, Y.-E. *J. Phys. Chem. B* **2003**, *107*, 5851.
(12) Arico, A. S.; Antonucci, P. L.; Modica, E.; Baglio, V.; Kim, H.; Antonucci, V. *Electrochim. Acta* **2002**, *47*, 3723.
(13) Hutchinson, J. M. Jr., *Platinum Met. Rev.* **1972**, *16*, 88.
(14) Hardeveld, R. V.; Hartog, F. *Surf. Sci.* **1969**, *15*, 189.
(15) Nashner, M. S.; Frenkel, A. I.; Somerville, D.; Hill, C. W.; Shapley, J. R.; Nuzzo, R. G. *J. Am. Chem. Soc.* **1998**, *120*, 8093.
(16) Nashner, M. S.; Frenkel, A. I.; Adler, D. L.; Shapley, J. R.; Nuzzo, R. G. *J. Am. Chem. Soc.* **1997**, *119*, 7760.
(17) Briggs, D.; Seah, M. P. *Practical Surface Analysis*; John Wiley & Sons: New York, 1990; Vol. 1.
(18) Yuvaraj, S.; Chang, T. H.; Yeh, C. T. *J. Catal.* **2004**, *221*, 466.
(19) Hwang, C. P.; Yeh, C. T. *J. Mol. Catal. A* **1996**, *112*, 295.
(20) Fronasiero, P.; Kaspar, J.; Montini, T.; Samto, V. D.; Psaro, R.; Recchia, S. *J. Mol. Catal. A* **2003**, *204*, 683. Huang, H. F. Effect of Calcination on Supported Platinum Catalysts, MS dissertation, National TsingHua University, Taiwan, 2003.
(21) Hwang, C. P.; Yeh, C. T. *J. Catal.* **1999**, *182*, 48.
(22) Hosokawa, S.; Kanai, H.; Utani, K.; Taniguchi, Y. I.; Saito, Y.; Imamura, S. *Appl. Catal. B* **2003**, *45*, 181.
(23) Mazzieri, V.; Coloma-Pascual, F.; Arcoya, A.; L'Argentiere, P. C.; Figoli, N. S. *Appl. Surf. Sci.* **2003**, *210*, 222.
(24) Crisafulli, C.; Scire, S.; Minico, S.; Solarino, L. *Appl. Catal. A* **2002**, *225*, 1.
(25) Koopman, P. G.; Kieboom, A. P. G.; Bekkum, H. V. *J. Catal.* **1981**, *69*, 172.
(26) Rouco, A. J.; Haller, G. L.; Oliver, J. A.; Kemball, C. J. *J. Catal.* **1983**, *84*, 297.
(27) From JCPDS data.